# Journal of Materials Chemistry B

Accepted Manuscript



This is an *Accepted Manuscript*, which has been through the Royal Society of Chemistry peer review process and has been accepted for publication.

Accepted Manuscripts are published online shortly after acceptance, before technical editing, formatting and proof reading. Using this free service, authors can make their results available to the community, in citable form, before we publish the edited article. We will replace this Accepted Manuscript with the edited and formatted Advance Article as soon as it is available.

You can find more information about *Accepted Manuscripts* in the **Information for Authors**.

Please note that technical editing may introduce minor changes to the text and/or graphics, which may alter content. The journal's standard <u>Terms & Conditions</u> and the <u>Ethical guidelines</u> still apply. In no event shall the Royal Society of Chemistry be held responsible for any errors or omissions in this *Accepted Manuscript* or any consequences arising from the use of any information it contains.





### **Journal Name**

### **ARTICLE**

## Targeting mitochondrial DNA with a two-photon active Ru (II) phenanthroline derivative

Received 00th January 20xx, Accepted 00th January 20xx

DOI: 10.1039/x0xx00000x

www.rsc.org/

Hui Wang<sup>a†</sup>, Xiaohe Tian<sup>b†</sup>, Lijuan Guan<sup>c</sup>, Qiong Zhang<sup>a</sup>, Shengyi Zhang<sup>a</sup>, Hongping Zhou<sup>a</sup>, Jieying Wu\*<sup>a</sup>, Yupeng Tian\*<sup>a,d</sup>

As a semi-autonomous organelle, eukaryotic mitochondrion possesses their individual DNA and protein synthesizing system. Therefore, the mitochondrial DNA-targeting probes are powerful tools to understand the functions in physiological processes. Herein, we report a novel of Ru (II) complex (HLRu) based on phenanthroline derivative to target mitochondrial DNA. The nonlinear optical properties study revealed a reverse nonlinear optical refraction character from self-focusing to self-defocusing response before and after complexation with Ru (II). Furthermore, the two-photon absorption and high biocompatibility of complex HLRu highlight their potential applications in biological processes. It was found that complex HLRu specifically binds with mitochondrial DNA in living cells and imaging of tissues with minimal autofluorescence. As a result, this complex HLRu probe offers a promising platform to directly monitor mitochondrial DNA in

### 1. Introduction

As a vital energy supplying organelle, mitochondria play significant roles in metabolism of cells, organs, tissues, as well as the whole living body. 1-4 Although, the number, size and morphology of mitochondria vary from organism to organism, their structural composition is usually same. Mitochondrial dysfunction affects the body homeostasis and causes neurodegenerative and neuromuscular disorders.<sup>5</sup> Noninvasive and real-time tracking of mitochondrial movements and morphological changes can help to elucidate the details of these processes and require efficient fluorescent probes. The biopolymer DNA is the primary carrier of all genetic information and mainly existed within nuclear region and mitochondrial inner membrane matrix in eukaryotic cells. Mitochondrial DNA (mtDNA) only takes a small portion of the DNA in a whole cell and it is entirely or largely autonomous with regard to their replication and translation. It is believed that mtDNA plays significant roles in female inheritance and ATPase subunit synthesizing. The commercial dye Mitotrackers, such as Rhodamine 123, MitoTracker Green FM, MitoTracker Red FM and MitoTracker Deep Red FM are available, whereas none of them are mitochondrial DNA specific. These commercial dyes also possess low photostability and small Stokes shifts, which also limit their

Recently, nonlinear microscopy techniques have provided new opportunities for biological imaging. 10,11 Two-photon microscopy (2PM) has become a crucial tool in bio-imaging applications, which employs excitation source at low energy near infrared (NIR) region. In contrast to one-photon microscopy (OPM) imaging techniques, 2PM facilitates spatial 3D localization reconstruction in deeper tissue without influence from endogenous fluorophore. 12,13 On the other hand, two-photon absorption (2PA) materials with large twophoton absorption cross section ( $\sigma$ ) values usually possess extended  $\pi$ -conjugated planar structures, which are often not compatible with biological specimens. Thus, the design and synthesis of novel fluorescent probes with large  $\sigma$  values and good biocompatibility is a fundamental and vital work for researchers.14

Transition metal ruthenium (d<sup>6</sup>) complexes with luminescent character have attracted arising attentions due to their desired photophysical properties, such as large Stokes shifts, pronounced photo-stability, color-tunable luminescence, and long emission lifetimes. 15,16 For example, Barton et al. reported a cell-penetrating peptide conjugated ruthenium complex, which achieved the entry into the nucleus.<sup>17</sup> Thomas et al. reported a dinuclear Ru (II) polypyride complex that functions as a structure-sensitive probe for the direct DNA labeling in vitro. 18 All these observations suggest that Ru (II) complexes have the potential to be used as subcellular markers.

Corresponding author. Fax: +86-551-63861279; Tel: +86-551-63861279 E-mail address: jywu1957@163.com; yptian@ahu.edu.cn

application for long-term tracking under laser confocal microscopy.<sup>8,9</sup> Moreover, most of them can only be used with onephoton microscopy (OPM) and short excitation wavelengths with shallow penetration depth, limiting their use in thick tissues. To circumvent these issues, alternative fluorescent dyes are needed that capable of noninvasive two-photon imaging, and less prone to photobleaching.

<sup>&</sup>lt;sup>a.</sup> Department of Chemistry, Key Laboratory of Functional Inorganic Materials Chemistry of Anhui Province, Anhui University, 230601, Hefei, P.R. China

<sup>&</sup>lt;sup>b.</sup> School of Life Science, Anhui University, 230601, Hefei, P.R. China

<sup>&</sup>lt;sup>a</sup> Department of Chemistry, University College London, WC1H0AJ, UK.

<sup>&</sup>lt;sup>t.</sup> State Key Laboratory of Coordination Chemistry, Nanjing University, Nanjing 210093. P. R. China.

<sup>†:</sup> These authors contributed equally to this work and should be considered co-first authors

Herein, we designed a novel 2P fluorescent mitochondrial probe (complex **HLRu**, in **Scheme 1**) based on imidazo [4, 5-f] [1, 10] phenanthroline. First, the phenothiazine group has a rich  $\pi$ -electron donating ability and high electron delocalization capability. Second, the alkyl chain can further influence the extent of electron delocalization and, consequently increase the solubility of the complex molecule. This in turn enables the use of biological-friendly solvents (e.g. PBS) in later long-term live cell experiments. Pemarkably, complex **HLRu** exhibits excellent photophysical properties in the NIR region comparing to its free ligand, such as exceptional nonlinear optical properties, large Stokes shifts, relatively long lifetimes and high photostability, as well as positive charge. More importantly, complex **HLRu** can interact with mitochondrial DNA *in vitro*.

$$\begin{array}{c} \text{Ru}(\text{phen})_2\text{Cl}_2\\ \text{NH}_4\text{PF}_6 \end{array} \qquad \begin{array}{c} \text{N}\\ \text{N}$$

Scheme 1 Synthetic routes for the ligand and its Ru (II) complex HLRu.

### 2. Experimental section

### 2.1 Materials and apparatus

All chemicals and solvents were dried and purified by standard methods. IR spectra (4000-400cm<sup>-1</sup>), as KBr pellets, were recorded on a Nicolet FT-IR 870 SX spectrophotometer. The <sup>1</sup>H-NMR spectra recorded on at 25°C using Bruker 400 Ultrashield spectrometer were reported as parts per million (ppm) from TMS (δ). MALDI-TOF mass spectra were performed on Bruker Autoflex III Smartbeam. Elemental analysis were carried out on a Perkin-Elmer 240 analyzer.

UV-vis absorption spectra were recorded on a SHIMADZU UV-3600 spectrophotometer. The fluorescence spectra were performed with use of a HITACHI F-2500 Spectrofluorophotometer. The concentration of sample solution was  $1.0\times10^{-5}$  mol/L. The two techniques for 2PA cross-sections were measured by two-photon excited fluorescence (2PEF) and Z-scan methods, respectively. The 2PA cross-section ( $\sigma$ ) were measured using the 2PEF method with the following equation: <sup>20</sup>

$$\sigma = \sigma_{\mathit{ref}} \, \frac{\Phi_{\mathit{ref}}}{\Phi} \, \frac{c_{\mathit{ref}}}{c} \, \frac{n_{\mathit{ref}}}{n} \, \frac{F}{F_{\mathit{ref}}}$$

Here, the subscripts ref stands for the reference molecule.  $\sigma$  is the 2PA cross-section value, c is the concentration of solution, n is the refractive index of the solution, F is the integrated area of the detected two-photon-induced fluorescence signal, and  $\Phi$  is the fluorescence quantum yield. The  $\sigma_{ref}$  value of reference is taken from the literature.  $^{21}$ 

The third-order nonlinear (NLO) optical properties of the samples in DMSO solution were obtained by the Z-scan method with a femtosecond laser piles and a Ti:sapphire system (680-1080 nm,10Hz, 140fs) as the light source. For time-resolved fluorescence measurements, the fluorescence signals were collimated and focused onto the entrance slit of a monochromator with the output plane equipped with a photomultiplier tube (HORIBA HuoroMax-4P). The decays were analyzed by 'least-squares'. The quality of the exponential fits was evaluated by the goodness of fit  $(\chi^2)$ .

### 2.2 Synthesis

# 2.2.1 Synthesis of 2-(10-hexyl-10H-phenothiazin-7-yl)-1H-imidazo [4,5-f][1,10] phenanthroline (HL)

A solution of 1,10-phenanthroine-5,6-dione  $^{22}$  (0.74 g, 3.5 mmol), 10-hexyl-10H-phenothiazine-3-carbaldehyde  $^{23}$  (1.09 g, 3.5 mmol) and ammonium acetate (5.75 g, 75 mmol) in acetic acid (75 mL) was refluxed for 4 h in nitrogen atmosphere. The solution was cooled down to room temperature, and then poured into water.  $K_2CO_3$  was added to adjust the pH to 7 under vigorously stirring. The generated yellow precipitation was washed with water and dichloromethane. Yield: 1.30 g (74%).  $^1\text{H-NMR}$  (d<sub>6</sub>-acetone, 400MHz, ppm): 0.86 (t, 3H), 1.33 (m, 4H), 1.50 (t, 2H), 1.84 (t, 2H), 4.03 (t, 2H), 6.98 (t, 1H), 7.21 (m, 3H), 7.75 (m, 2H), 8.06 (m, 1H), 8.16 (m, 1H), 8.91 (d, 2H), 9.03 (m, 2H). IR (KBr, cm $^{-1}$ ): 2924, 2852, 1606, 1568, 1466, 1415, 1394, 1247, 735. MS: 502.36[M+1] $^+$ . Anal. Calc. for  $C_{37}H_{27}N_5S$ : C, 74.22; H, 5.43; N, 13.96. Found: C, 74.31; H, 5.41; N, 13.99.

### 2.2.2 Synthesis of complex HLRu

A mixture of  $[Ru(phen)_2Cl_2]^{24}$  (0.26 g, 0.5 mmol), HL (0.25 g, 0.5 mmol) and methanol (60 mL) was refluxed for 12 h to give a clear red solution. After most methanol was removed by evaporation, a red precipitation was obtained by the dropwise addition of aqueous NH<sub>4</sub>PF<sub>6</sub> solution. The product was purified by column chromatography (silicagel, 50:1 dichloromethane /methanol) to form a red solid. Yield: 0.28 g (45%). <sup>1</sup>H-NMR (400MHz, d<sub>6</sub>-acetone, ppm): 0.85 (t, 3H), 1.31 (s, 4H), 1.50 (m, 2H), 1.83 (m, 2H), 4.03 (t, 2H), 6.99 (t, 1H), 7.12 (d, 1H), 7.23 (t, 1H), 7.49 (m, 5H), 7.81 (m, 4H), 7.96 (s, 1H), 8.18 (d, 1H), 8.28 (m, 2H), 8.42 (m, 7H), 8.79 (d, 4H), 9.07 (d, 2H). IR (KBr, cm<sup>-1</sup>): 2927, 1603, 1579, 1451, 1427, 1300, 1251, 1056, 838, 721, 557, 521. MS: 960.71 [M-2PF<sub>6</sub>]<sup>+</sup>. Anal. Calc. for  $C_{55}H_{43}N_9F_{12}P_2RuS$ : C, 52.72; H, 3.46; N, 10.06; Found: C, 52.85; H, 2.43; N, 10.02.

### 2.2.3 X-ray ctystallograhy

The X-ray diffraction measurements were performed on a Bruker SMART CCD area detector using graphite monochromated Mo- $K_{\alpha}$  radiation ( $\lambda=0.71069$  Å) at 298(2)K. Intensity data were collected in the variable  $\omega$ -scan mode. The structures were solved by direct methods and difference Fourier synthesis. The non-hydrogen atoms were refined anisotropically and hydrogen atoms were introduced geometrically. Calculations were performed with SHELXTL-97 program package.  $^{25}$ 

### 2.2.4 Computational details

Optimizations were carried out with B3LYP [LANL2DZ] without any symmetry restraints, and the TD-DFT {B3LYP[LANL2DZ]}

Journal Name ARTICLE

calculations were performed on the optimized structure. All calculations, including optimizations and TD-DFT, were performed with the G03 software. Geometry optimization of the singlet ground state and the TD-DFT calculation of the lowest 25 singlet-singlet excitation energies were calculated with a basis set composed of 6-31G for C H N S O atoms and the Lanl2dz basis set for Ru atoms were download from the EMSL basis set library.

### 2.2.5 DNA-binding properties

All experiments dealing with the interaction of HLRu with calf thymus (ct-DNA) were conducted in buffer solution (pH 7.4, 50 mM Tris-HCl, 50 mM NaCl). The solutions of ct-DNA gave ratios of UV absorbance at 260 nm to that at 280 nm of about 1.9:1, indicating that the DNA was sufficient free of protein. The concentration per nucleotide of DNA was determined spectrophotometrically by assuming  $\varepsilon_{260 \text{ nm}}$ =6600 M cm<sup>-1</sup>. The absorption titration with ct-DNA was by keeping the concentration of HLRu constant while varying the DNA concentrations. The competitive binding of ethidium bromide (EB) to the DNA with HLRu was carried out by measuring EB emission ( $\lambda_{ex}$ =537nm) while keeping [DNA]/[EB]=1 constant with varying HLRu concentrations. Viscosities of the DNA were measured on an Ubbelohde viscometer, immersed in a thermostated water-bath maintained at 32.14±0.05°C. Data were presented as  $(\eta/\eta_0)^{1/3}$  vs the ratio of the concentration of **HLRu** to that of the DNA, where  $\eta$  and  $\eta_0$  are the viscosities of DNA solutions in the presence and absence of complex HLRu, respectively. Viscosity values were calculated from the observed flow times of DNA containing solutions (t) corrected for that of buffer alone ( $t_0$ ),  $\eta=t-t_0$ .

### 2.2.6 Cell Imaging

HepG2 cells were seeded in 24-well glass bottom plates (Corning®, P2415HN) at the density of  $1\times10^4$  cells per well and grew for 96 hours. For live cell imaging, the culture medium was DMEM supplemented with 10% FCS, penicillin and streptomycin, L-glutamine and Fungizone at 37°C in an atmosphere of 5% CO<sub>2</sub> and 95% air for 30 min incubation. The cells were then washed with PBS (2×2 ml per well) and 2 ml of PBS was added to each well. The cells were imaged using confocal laser scanning microscopy.

### 2.2.7 Microscopy

Cells were imaged on a ZEISS LSM 710 META confocal laserscanning microscope with 63x oil lens. A Coherent Chameleon pulsed infrared multiphoton laser was used for two-photon imaging (760 nm) check. For the real-time imaging, live cell imaging, an incubation chamber was connected to ZEISS temperature control unit 37 °C and CO<sub>2</sub> controller and proper humidity (1-2 hours before the experiment was allowed for the stabilization of temperature and CO<sub>2</sub> concentration). For complex **HLRu**, the excitation wavelength of 760 nm was used and the emission was measured at 590-620 nm. Co-staining was performed by incubating cells with 2 µM Syto9 ( $\lambda_{ex}$ =488 nm,  $\lambda_{em}$ =500–530 nm) for 15 min and 1  $\mu$ M Hoechst 33342 ( $\lambda_{ex}$ =405 nm,  $\lambda_{em}$ =420-450 nm) for 15 min and 1  $\mu$ M Mitotracker ( $\lambda_{ex}$ =579 nm,  $\lambda_{em}$ =585–610 nm) and 1  $\mu$ M ER-Tracker ( $\lambda_{ex}$ =488 nm,  $\lambda_{\rm em}$ =500–520 nm) for 30 min. For transmission electron microscopy (TEM), HepG2 cells were incubated with complex HLRu (30 min) then fixed in 3% glutaraldehyde and dehydrated in ethanol. TEM

samples were sectioned in Araldite resin by microtome and examined on a FEI Tecnai instrument operating at 80 kV equipped with a Gatan 1 k CCD Camera. Imaging data acquisition and processing were performed using Zeiss LSM Image Browser, Zeiss LSM Image Expert and Image J.

### 2.2.8 MTT Cytotoxicity assays

To ascertain the cytotoxic effect of HLRu treatment over a 24h period, the 5-dimethylthiazol-2-yl-2,5-diphenyltetrazolium bromide (MTT) assay was performed. HepG2 cells were grown to ~70% confluence in 96-well plates before treatment. Prior to the compounds' treatment, the growth medium was refreshed, and complex HLRu was first dissolved in DMSO to 1 mM and then diluted twice by DMEM cell culture medium to obtain the final concentrations. The treated cells were incubated for 24 h at 37 °C and under 5% CO<sub>2</sub>. Subsequently, the cells were treated with 5 mg/mL MTT solution (10 μL/well) and incubated for an additional 4 h (37 °C, 5% CO<sub>2</sub>). Then, MTT solution was removed and the formazan crystals were dissolved in DMSO (100 µL/well). The absorbance at 490 nm was recorded. The cell viability (%) was calculated according to the following equation: cell viability % =OD<sub>490</sub> (sample)/OD<sub>490</sub> (control)  $\times 100$ , where OD<sub>490</sub> (sample) represents the optical density of the wells treated with various concentrations of the compounds and  ${\rm OD}_{490}$  (control) represents that of the wells with only DMEM + 10% FCS. Three independent trials were conducted, and the averages and standard deviations are plotted. The reported cell survival percent are relative to untreated control cells.

### 2.2.9 Fresh tissue staining

Specific pathogen Free (SPF) KM (Kunming) mouse (male, two month, 18-22g) was terminally anaesthetised and transcardially perfused with phosphate buffered saline (PBS) 0.1M pH 7.4. The brain was extracted and the tissues were then snap frozen in liquid nitrogen cooled isopentane. Fresh frozen organs from PBS-perfused animals were sectioned at  $100~\mu m$  in the sagittal plane using a cryostat (Leica 1950). The fresh tissue incubated with  $10~\mu M$  HLRu solution for 30 minutes at 37 °C in 95% air 5% CO2, then washed with PBS buffer 3 times. Tissue was mounted cover-slipped using an aqueous Prolong Diamond Antifade medium with DAPI (Life Technology S36939), and imaged directly using a Zeiss LSM 710 upright confocal system.

Note: All procedures involving animals were approved by and conformed to the guidelines of the Anhui University Animal Care Committee. We have taken great efforts to reduce the number of animal used in these studies and also taken effort to reduce animal suffering from pain and discomfort.

### 3. Results and discussion

### 3.1 Synthesis and characterization

The synthetic route of the complex is shown in **Scheme 1**. The ligand **HL** was synthesized by coupling 1,10-phenanthroine-5,6-dione with 10-hexyl-10H- phenothiazine-3-carbaldehyde according to protocols reported by Steck and Day.<sup>27</sup> The complex **HLRu** was prepared by direct reaction of [Ru(phen)<sub>2</sub>Cl<sub>2</sub>] with **HL** in methanol, and purified by column chromatography on silica gel with

dichloromethane /methanol (v/v = 50:1) as eluent. All compounds were characterized by elemental analyses, IR, MOLDI-TOF-MS and NMR spectral techniques (**Fig S1-S4**). Meanwhile, the crystal structure of **HL** was obtained. The crystal structure of **HL** is shown in

Fig S5. The unit cell, data collection, and refinement parameters are demonstrated in Table S1. Selected bond lengths and angles are given in Table S2.

**Table 1.** Two-photon absorption ratio  $\beta$ , cross section  $\sigma$  and nonlinear parameter test results of **HL** and complex **HLRu**.

Compds	Maximum nonlinear absorption wavelength ( nm )	β(cm/W)	σ(GM) <sup>[1]</sup>	$\gamma$ (cm <sup>2</sup> /W)	χ <sup>(3)</sup> (esu)	$R_e\left(\chi^{(3)}\right)$ (esu)	$I_m\left(\chi^{(3)}\right)$ (esu)
HL	710	3.69×10 <sup>-3</sup>	171.5	4.05×10 <sup>-16</sup>	1.08×10 <sup>-8</sup>	2.09×10 <sup>-14</sup>	1.08×10 <sup>-8</sup>
HLRu	760	5.37×10 <sup>-3</sup>	236.5	1.71×10 <sup>-14</sup>	1.66×10 <sup>-8</sup>	8.86×10 <sup>-13</sup>	1.66×10 <sup>-8</sup>

[1] 1GM=1×10<sup>-50</sup> cm<sup>4</sup>s/photon

# 3.2 Linear absorption, TD-DFT calculation and single-photon excited fluorescence (SPEF)

The photophysical data of the compounds (in five solvents with different polarities at a concentration  $c=1.0\times10^{-5} \, \text{mol/L}$ ) are collected in **Table S3** (corresponding figures are given in supporting information).

As seen in **Fig 1(a)**, the linear absorption spectrum of **HL** exhibits three bands between 250 and 410 nm. The low energy band originates from the intramolecular charge transfer (ICT) transition, while the highest energy band is assigned to the  $\pi_{\text{phenothiazine}}$  transitions. A moderate intense absorption at 317 nm is assigned to the  $\pi$ - $\pi$ \* transitions. On the other hand, the complex **HLRu** exhibits the absorption bands in the range of 250-550 nm. Different from **HL**, in this case, the higher energy band was assigned to the  $\pi$ - $\pi$ \* transition or ICT transition, while the lower energy band was tentatively assigned to metal-to-ligand charge transfer (MLCT) Ru<sub>d $\pi$ </sub>-L<sub> $\pi$ \*</sub> transitions, <sup>27</sup> as confirmed by TD-DFT calculations (**Fig S8 and Table S4**, Supporting information).

As shown in both **Fig S6** and **Table S3**, a weak solvatochromism was observed in the ICT absorption bands, indicating that the dipoles of the compounds are different between their ground and excited states.<sup>29</sup>

Interestingly, upon increasing the solvent polarity, the fluorescence spectra of HL showed a red shifts, together with a monotonically increase intendency in the Stokes shift, this can be explained by the fact that the excited state may possess a higher polarity than the ground state, since the solvatochromism is associated with a lowering of the energy levels, an increased dipoledipole interaction between the solute and solvent leads to a lowering of the energy level, whereas no obvious changes were observed in complex HLRu (Fig S7 and Table S3). The fluorescence intensity of HL and complex HLRu both decreased along the increase of the solvent polarity (Fig S7). The fluorescence lifetimes of the ligand HL and complex HLRu in aprotic solvents are prolonged with the increase of solvent polarity. In protic solvents, HL and complex HLRu exhibited shorter lifetimes, especially in ethanol for HL, in which the  $\tau$  value is less than 0.2 ns. Moreover, the lifetime of complex HLRu is longer than that of HL, may be due to significant vibronic coupling between MLCT emitting state and higher lying triplet  $\pi \rightarrow \pi^*$  states.<sup>30</sup>

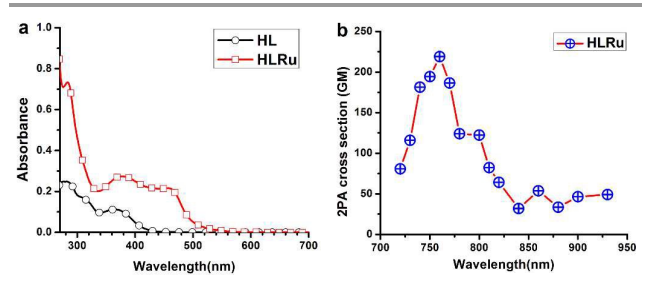


Fig. 1 (a) Linear absorption spectra of HL and HLRu in CH<sub>3</sub>CN solution (c= $1.0 \times 10^{-5}$  mol/L). (b) Two-photon absorption cross sections of HLRu in DMSO solution (c= $10^{-3}$  mol/L).

### 3.3 Two-photon absorption cross-sections

The two-photon excited fluorescence (2PEF) spectra of **HLRu** in DMSO were recorded at its maximum excitation wavelength with a pulse duration of 140 fs at 300 mW. As shown in **Fig S9**, the 2PEF exhibits logarithmic plots of the fluorescence intergral versus input power. The logarithmic plots has slope of 2.18 as the input laser power is increased, suggesting a two-photon excitation mechanism. No linear absorption was observed in the range from 500 nm to 800 nm, so the emission excited by 760 nm laser wavelength can be attributed to the 2PEF mechanism. As shown in **Fig 1(b)**, **HLRu** displays 2PA activity in the range of 720-930 nm in DMSO. The 2PA cross sections of **HLRu** were determined by investigating its two-photon excited fluorescence using rhodamine B as the reference. The maximum 2PA cross section for **HLRu** is approximately 219 GM units at 760 nm, which is larger than those of reported Ru (II) complexes.<sup>31</sup>

To further confirm the 2PA performances, the 2PA coefficient  $\beta$  and 2PA cross-section  $\sigma$  of **HL** and **HLRu** were measured by the Z-scan technique.  $^{32-34}$  The thermal heating of all samples with high repetition rate of the pulse femtosecond laser was removed by using a mechanical chopper running at 10 Hz. An incident average power of 200 mW was adjusted by a Glan prism. A 1 mm cell of the sample  $(1.0\times10^{-3}\,\text{mol/L}$  in DMSO) was put in the light path.

The nonlinear 2PA coefficient  $\beta$  (in units of cm/GW) and the molecular 2PA cross-section  $\sigma$  (in units of cm<sup>4</sup>s/photon) have been

Journal Name ARTICLE

plotted in **Table 1**. In **Fig 2**, the open aperture transmittance are symmetric with respect to the focus (z=0). The obvious minimum transmittance unambiguously indicated a large nonlinear absorption, which is attributed to 2PA effect because the ligand **HL** and its complex **HLRu** showed no linear absorption after 500 nm. As showed in **Table 1**, two-photon absorption cross section of the complex **HLRu** is much larger than its free ligand **HL**. It was proved that the NLO response was well consistent with the extended  $\pi$ -electron delocalization in the complex molecule.

Meanwhile, the third-order nonlinear refractive index  $(\gamma)$  was determined by the close aperture Z-scan technique. 35-37 As shown in Fig 2, the curve indicates that the ligand HL has a positive sign for the refractive nonlinearity, which gives rise to the self-focusing behavior. Interestingly, a reversed nonlinear optical refraction was observed from self-focusing to self-defocusing response after the complexation. 38,39 Moreover, a dramatic increase of both nonlinear refraction and nonlinear absorption in complex HLRu was detected comparing to those in the free ligand HL (Table 1), suggesting that the complex HLRu possesses a large third-order nonlinear susceptibility. Considering the remarkable value of  $\chi^{(3)}$  that is caused by highly delocalized  $\pi$ -electronic configuration and large intrinsic polarizability, the complex HLRu is a good candidate as third-order nonlinear optical materials. Importantly, the strong third-order nonlinear optical response occurs within the near-infrared region, encouraging us to further investigate its applications in biology.

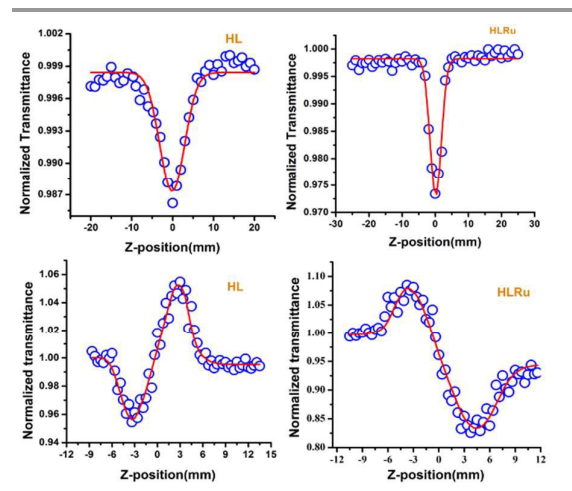


Fig. 2 The open (up) and close (bottom) aperture Z-scan data at 710, 760 nm for HL and complex HLRu in DMSO at  $1.0\times10^{-3}$  mol/L, respectively. The circle rings represent the experimental data and the solid curve is the theoretical data.

### 3.4 DNA binding properties

UV-vis absorption spectroscopy is an effective method to examine the binding mode of small molecules with DNA. <sup>40</sup> The binding mode of **HLRu** with ct-DNA was primarily studied by UV-vis absorption. As shown in **Fig S10a**, upon increasing concentrations of DNA, the absorption band at 260 nm displayed clear hypochromisties with hypochromisms H%, as defined by H% = 100 ( $A_{free}$ - $A_{bound}$ )/ $A_{free}$ , for the  $\pi$ - $\pi$ \* band at 260 nm was found to be 37.3%. The intrinsic binding constant  $K_b$  of **HLRu** with DNA was evaluated to be 2.99

 $\times 10^5$  M<sup>-1</sup>, which indicates the considerable intercalative binding intensity of **HLRu** to DNA.

The DNA binding property of **HLRu** is also discussed *via* fluorescent spectral analysis, based on the competitive binding between EB and **HLRu** with ct-DNA. From **Fig S10b**, we can see that EB molecules bound by ct-DNA gave strong fluorescence emission with maximum emission intensity at 597 nm. Under the increasing addition of **HLRu**, the fluorescent intensity of EB was gradually decreased. This indicates that there existed competitive binding between **HLRu** and EB, which suggests the intercalative binding mode of **HLRu** with DNA. The linear Stern-Volmer quenching constant K was calculated to be 4.33.

To further clarify the nature of the interactions between **HLRu** and DNA, viscosity measurements were carried out. As shown in **Fig S10c**, the relative viscosity of ct-DNA bound with the **HLRu** increased with increasing complex concentration similarly to the behavior of some known DNA intercalators, indicative of a classical intercalation of the complex to the DNA.

Equilibrium Dialysis Experiments may offer the opportunity to examine the enantioselectivity of the complex binding to DNA. According to the proposed the binding model, 41 the  $\Delta$  enantiomer of the complex, a right handed propeller-like structure, will display a greater affinity than the  $\Lambda$  enantiomer with the right handed ct-DNA helix, due to the appropriate steric matching. The CD spectrum of ct-DNA exhibits a positive band at 277 nm due to base stacking and a negative band at 248 nm due to the helicity of DNA. In the presence of HLRu an increase in the molar eliplicity values of the both positive and negative band of the ct-DNA is observed (Fig S10d). Those significant changes indicate conformational changes and unwinding of DNA base pairs with destabilization of the DNA double helix, which is consistent with DNA intercalation mode suggested above. Combined with the results from the above mentioned spectral analyses, the interaction between HLRu and DNA is confirmed to be an intercalative binding mode.

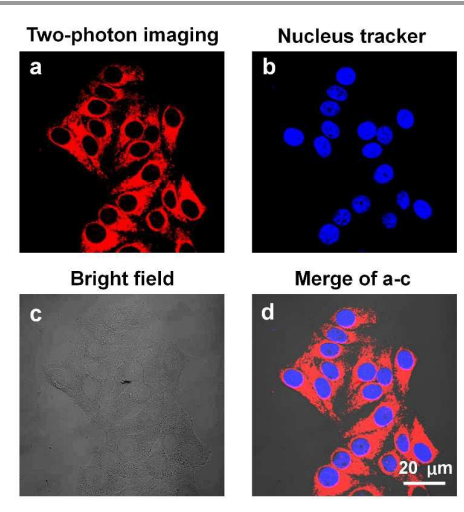


**Fig. 3** Two-photon images of living cells incubated with 10 μM **HLRu** for 30 min and then further incubated with Hoechst 33342 for 15min. (a) Two-photon images of **HLRu** (b) Fluorescence images of Hoechst 33342. (c) Bright filed. (d) Merge images of a-c.

### 3.5 Two-photon microscopy biological imaging application

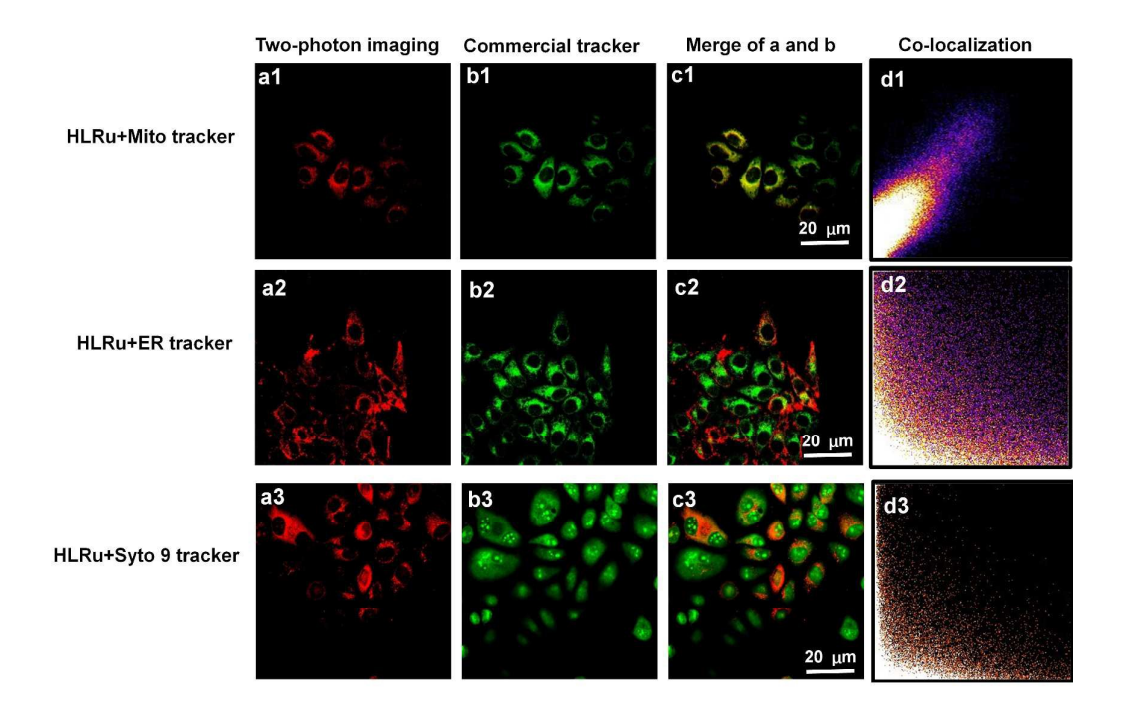
High cell viability is essential for fluorescent probes in their biological applications. As Ru complexes have relatively low toxicity in live cells, complex **HLRu** was chosen for further live cell studies, also due to its larger 2PA cross-section and longer fluorescent lifetime. HepG2 cells was firstly incubated with 10  $\mu$ M of **HLRu** for 30 minutes and imaged directly without the fixation. The cytotoxicity of complex **HLRu** in different cancer cells (HepG2, MCF-7 and A549 cells) was evaluated by MTT assay. The result elucidates that **HLRu** generally present low toxicity in living cell under the conditions applied (**Fig S11**).

Clear intracellular fluorescence was observed in live cell imaging by confocal microscopy. As respected, the two-photon signal of complex **HLRu** was more distinct than that with one-photon excitation (**Fig S12 and Fig 3**). As shown in **Fig 3**, the Ru (II) stained structures are tubule-like and emitted only from cell cytoplasm, while DIC (Differential interference contrast) micrograph confirmed good cell shapes and morphology. The co-staining with Hoechst 33342 further excluded the localization of complex **HLRu** in nuclear region.

To determine the possible mechanism of complex HLRu's cell entry, HepG2 were incubated with 10 μM complex HLRu for 30 min at 4 °C, then washed and imaged directly. In this case (Fig S13), weak fluorescence was detected, highly indicating that HLRu is membrane impermeable molecules and enters cells *via* a temperature-dependent pathway (e.g. endocytosis and active transport). As widely accepted, the most common energy-dependent method for eukaryotic cells to internalize extracellular materials is endocytosis. In order to examine if complex HLRu enter cell *via* endocytosis, cells were incubated with HLRu and several well-defined inhibitors of this process. The cell internalization was then assessed by the extent of resultant cytoplasm staining by 2PM (Fig S14). A relative intracellular fluorescent intensity was measured and

plotted (**Fig S14**) after the treatment of the inhibitors, the general endocyotsis inhibitors, chloroquine and ammonium chloride (two lysosomotropic agents) <sup>42</sup> or chlorpromazine the inhibitor of clathrin-mediated endocytosis. <sup>43</sup> The ability of **HLRu** to function as a mitochondrial probe was clearly affected, indicating that complex **HLRu** was taken by cells *via* endocytic pathway. However, neither colchicines or nocodazole, which disrupt the polymerization of microtubules and consequently prevent the trafficking of endosomal compartments, <sup>44</sup> showed any inhibition of uptake. Moreover, the ATP synthesis inhibitors, 2-deoxy-D-glucose (DOG), reduced the cellular uptake of **HLRu** to 82.60%. Thus, we came to the conclusion that the pathway by which complex **HLRu** enters HepG2 cells is energy-dependent endocytosis.

Except for cell nucleus, DNA also abundantly exists in mitochondrial inner membrane matrix, which is essential for the coding of functional ATPase subunit. Therefore, to fully understand the intracellular localization of complex HLRu, a co-localization experiment within the mitochondria was performed (Mitotracker Red CMXRos, MTR). Endoplasmic reticulum (ER-Tracker<sup>TM</sup>) and SYTO 9 co-localization were conducted as a control here (Fig 4). The fluorescence of complex HLRu overlapped with that of MTR with a Pearson's coefficient Rr = 0.88, but little overlapping with ER-Tracker (Rr = 0.02) and even no overlapping with Hoechst and Syto9 (Fig 4). To further confirm the selectivity of HLRu to DNA, the digest test of deoxyribonuclease (DNase) was performed (Fig 5). Upon treatment with DNase (Fig 5a), in which DNA was hydrolyzed while RNA kept intact, the two-photon fluorescence of HLRu in cytoplasm sharply diminished. The result indicated that **HLRu** prefer to DNA in the complex internal environment of cells. It is strongly suggested that complex HLRu localizes to the mitochondria and highly binds with mitochondrial DNA. This result was not unexpected as HLRu is positively charged, which is essential for mitochondrial targeting probes. 45,46



Journal Name ARTICLE

Fig. 4 Two-photon images of HepG2 cells co-labeled with HLRu and Mito tracker (a1-d1), ER tracker (a2-d2), Syto 9 tracker (a3-d3), respectively.

In addition to fluorescent microscopy, Ru (II) polypyridyl compounds may function as contrast agents in transmission electron microscopy (TEM) imaging for the analysis of cellular sections courtesy of the electron-dense Ru(II) metal centre. 47,48 Compared to the non-treated cells (Fig 6c), Fig 6a showed that complex HLRu was located throughout the cell cytosol, but found in much higher concentration within mitochondria inner space and no colocalization with nucleus. Although without osmium tetraoxide, the TEM micrographs showed less membrane contrast, the mitochondria of HepG2 cells were clearly stained by complex HLRu after the incubation (Fig 6b). These findings are again in agreement with the two-photon microscopy imaging, and cooperate with DNA *in vitro* studies, all strongly suggesting that complex HLRu has a superior interaction with intracellular DNA that are located within mitochondria inner matrix in live cells.

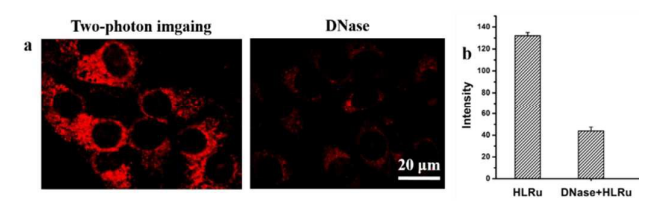


Fig. 5 (a) Live-cell staining and DNase digest experiments with complex HLRu in HepG2. (b) The relative two-photon fluorescence intensity of HLRu and DNase+HLRu.

To further assess the performance of **HLRu** for bioimaging applications, we investigated the applicability of this complex for tissue imaging. The tissue slice samples were prepared from mouse organ (brain) under usual fixative conditions, which were stained by incubating with **HLRu** for 30 min, then incubated with Hoechst 33342 for 15 min, and washed with PBS buffer. The 2PM images of the organ stained with **HLRu** show strong fluorescence when excited at 760 nm (**Fig S15**). The data indicate that complex **HLRu** display good capability of tissue imaging by using two-photon fluorescence microscopy, in accord with its good two-photon fluorescence properties.

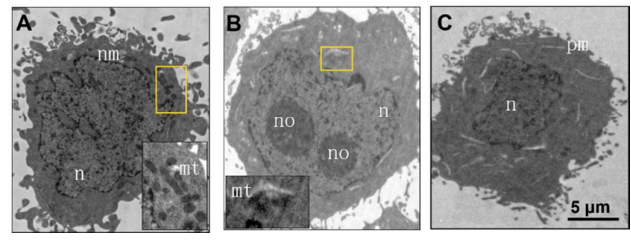


Fig. 6 Cellular localization of complex HLRu characterized by transmission electron microscopy. (A) TEM microscopy of HepG2 cells incubated with HLRu and stained with osmium tetroxide. (B) TEM microscopy of HepG2 cells incubated with HLRu and non-stained with osmium tetroxide. (C) TEM microscopy of HepG2 cells incubated without HLRu stained with osmium tetroxide. Abbreviations: n=nucleus, nm=nuclear membrane, mt= mitochondria, no= nucleolus, pm=plasma membrane.

### 4. Conclusion

In summary, a novel Ru(II) complex has been designed and synthesized. The NLO studies demonstrated that the Ru(II) complex possesses much large 2PA cross section and remarkable value of  $\chi^{(3)}$ in the near-IR range comparing to its free ligand. Interestingly, the ligand HL exhibited a reversed nonlinear optical refraction from self-focusing to self-defocusing response after complexating with Ru(II). At present finding, the strong near-IR NLO response, as well as low toxicity of the Ru(II) complex make it to be promising applications in biology. The in vitro binding assay, two-photon confocal microscopy and transmission electron microscopy elucidated that complex HLRu enters cells via energy-dependent endocytosis, binds with mitochondrial DNA in live cells and tissues imging. Due to its low cytotoxicity, large 2PA cross section and efficient mitochondrial DNA staining, complex HLRu is believed to have great potential as biocompatible dyes for mitochondrial DNA in living cells under 2PM imaging. Current results have provided a platform for the design of new 2PM bioimaging probe to target DNA in mitochondria.

### **Acknowledgment**

This work was supported by grants from the National Natural Science Foundation of China (51372003, 21271004, 51432001 and 21271003, 21275006), China Postdoctoral Science Foundation (2015M571912), Ministry of Education Funded Projects Focus on returned overseas scholar, Program for New Century Excellent Talents in University (China) and the Higher Education Revitalization Plan Talent Project (2013).

### References

- M. Y. Wu, K. Li, Y. H. Liu, K. K. Yu, Y. M. Xie, X. D. Zhou and X. Q. Yu, *Biomaterials.*, 2015, 53, 669-678.
- N. Jiang, J. L. Fan, F. Xu, X. J. Peng, H. Y. Mu, J. Y. Wang and X. Q. Xiong, *Angew. Chem.*, 2015, 127, 2540-2544.
- 3 Y. C. Chen, C. C. Zhu, J. J. Cen, Y. Bai, W. J. He and Z. J. Guo, Chem. Sci., 2015, 6, 3187-3194.
- 4 X. X. Kong, F. Y. Su, L. Q. Zhang, J. Yaron, F. Lee, Z. W. Shi, Y. Q. Tian and D. R. Meldrum, *Angew. Chem. Int. Ed.*, 2015, **54**, 12053-12057.
- 5 Roola, N. Kumar, V. Bhalla and M. Kumar, *Chem. Commun.*, 2015, **51**, 15614-15628.
- K. Q. Qiu, H. Y. Huang, B. Y. Liu, Y. K. Liu, P. Y. Zhang, Y. Che,
   L. J. Ji and H. Chao, J. Mater. Chem. B., 2015, 3, 6690-6697.
- 7 Y. H. He, X. Lu, H. Wu, W. W. Cai, L. Q. Yang, L. Y. Xu, H. P. Sun and Q. P. Kong, *Neurobiology of Aging.*, 2014, 35, 1779e1-1779e4.
- 8 M. H. Lee, N. Park, C. Yi, J. H. Han, J. H. Hong, K. P. Kim, D. H. Kang, J. L. Sessler, C. Kang and J. S. Kim, J. Am. Chem. Soc., 2014, 136, 14136-14142.
- G. Zhang, J. J. Gruskos, M. S. Afzal and D. Buccella, *Chem. Sci.*, 2015, 6, 6841-6846.
- 10 C. Xu and F. W. Wise, Nat. Photonics., 2013, 7, 875-82.
- 11 D. L. Ma, H. Z. He, K. H. Leung, D. S. H. Chan and C. H. Leung. Angew. Chem. Int. Ed., 2013, 52, 2-19.
- 12 H. M. Kim and B. R. Cho, Chem. Rev., 2015, 115, 5014-5055.

- 13 B. Dumat, G. Bordeau, E. F. Paul, F. M. Betzer, N. Saettel, G. Metge, C. F. Debuisschert, F. Charra and M. P. T. Fichou, J. Am. Chem. Soc., 2013, 135, 12697-12706.
- 14 F. Miao, W. J. Zhang, Y. M. Sun, R. Y. Zhang, Y. Liu, F. Q. Guo, G. F. Song, M. G. Tian and X. Q. Yu, Biosensors and Bioelecttonics., 2014, 55, 423-429.
- 15 Q. Zhao, C. H. Huang and F. Y. Li. Chem. Soc. Rev., 2011, 40, 2508-2524.
- 16 Q. Zhao, F. Y. Li and C. H. Huang, Chem. Soc. Rev., 2010, 39, 3007-3030.
- 17 C. A. Puckett and J. K. Barton, J. Am. Chem. Soc., 2009, 131, 8738-8739.
- 18 M. R. Gill, J. Garica-Lara, S. J. Foster, C. Smythe, G. Battaglia and J. A. Thomas, *Nat. Chem.*, 2009, 662-667.
- 19 W. C. Xu, J. R. Zuo, L. L. Wang, J. N. Ji and H. Chao, *Chem. Commun.*, 2014, **50**, 2123-2125.
- 20 C. Xu and W. W. Webb. J. Opt. Soc. Am. B., 1996, 13, 481-491.
- 21 M. A. Albota, C. Xu and W. W. Webb. Applied. Optics., 1998, 37, 7352-7356.
- 22 H. H. Xu, X. Tao, Y. Q. Li, Y. Z. Shen and Y. H. Wei. Polyhedron., 2012, 33, 347-352.
- 23 X. Q. Zhang, Z. G. Chi, J. Y. Zhang, H. Y. Li, B. J. Xu, X. F. Li, S. W. Liu, Y. Zhang and J. R. Xu, J. Phys. Chem. B., 2011, 115, 7606-7611.
- 24 K. P. Pankaj, G. B. D. Michael and D. Dipankar. New. J. Chem., 2003, 27, 197-201.
- 25 G. M. Sheldrick. SHELXTL97, Program for Crystal Structure Solution; University of Göttingen: Göttingen. Germany. 1997.
- 26 M. J. Frisch, G. W. Trucks, H. B. Schlegel, G. E. Scuseria, M. A. Robb, J. R. Cheeseman, et al. Gaussian 03 (Revision B.04), Gaussion, Inc. Wallingford, CT, 2004.
- 27 C. S. Devi, D. A. Kumar, S. S. Singh, N. Gabra, N. Deepika, Y. P. Kumar and S. Satyanarayana, Eur. J. Med. Chem., 2013, 64, 410-421.
- 28 H. G. Zhang, X. T. Tao, K. S. Chen, C. X. Yuan, S. N. Yan and M. H. Jiang, *Chinese. Chem. Lett.*, 2011, **22**, 647-650.
- 29 H. Y. Woo, B. Liu, B. Kohler, D. Korystov, A. Mikhailovsky and G. C. Bazan, J. Am. Chem. Soc., 2005, 127, 14721-14729.
- I. M. Dixon, E. Lebon, P. Sutra and A. Igau, Chem. Soc. Rev., 2009, 38, 1621-1634.
- 31 J. P. Liu, Y. Chen, G. Y. Li, P. Y. Zhang, C. Z. Jin, L. L. Zeng, L. N. Ji and H. Chao, *Biomaterials.*, 2015, **56**, 140-153.
- 32 M. Sheik-Bahae, A. A. Said, T. H. Wei, D. J. Hagan and S. E. W. Van, *IEEE. J. Quantum. Electron.*, 1990, 26, 760-769.
- 33 W. Zhao and P. Paltty-Muhoray, *Appl. Phys. Lett.*, 1994, **65**, 673-675.
- 34 S. L. Li, J. Y. Wu, Y. P. Tian, Y. W. Tang, M. H. Jiang and H. K. Fun, Opt. Mater., 2006, 28, 897–903.
- 35 K. K. Nagaraja, S. Pramodini, A. S. Kumar, H. S. Nagaraja, P. Poornesh and D. Kekuda, *Opt. Mater.*, 2013, **35**, 431-439.
- 36 J. Y. Tan, R. Li, D. D. Li, Q. Zhang, S. L. Li, H. P. Zhou, J. X. Yang, J. Y. Wu and Y. P. Tian, *Dalton. Trans.*, 2015, 44, 1473-1482.
- 37 T. Geethakrishnan and P. K. Palanisamy, Opt. Commun.,
- 2007, **270**, 424-432.

  38 I. Guezguez, A. Ayadi, K. Ordon, K. Iliopoulos, D. G. B. Ranzea,

  A. Migalska-7alas, M. M. Janusik, A. F. Ghayoury, and B.
- A. Migalska-Zalas, M. M. Janusik, A. E. Ghayoury and B. Sahraoui, *J. Phys. Chem. C.*, 2014, **118**, 7545-7453.
- 39 Z. H. Shi, Y. S. Zhou, L. J. Zhang, S. U. Hassan and N. N. Qu, *J. Phys. Chem. C.*, 2014, **118**, 6413-6422.
- S. Anbu, S. Kamalraj, B. Varghese, J. Muthumary and M. Kandaswamy, *Inorg. Chem.*, 2012, 51, 5580-5592.
- 41 H. R. Zhang, Y. C. Liu, T. Meng, Q. P. Qin, S. F. Tang, Z. F. Chen, B. Q. Zou, Y. N. Liu and H. Liang, *Med. Chem. Commun.*, 2015, 6, 2224-2231.
- 42 H. K. Ziegler and E. R. Unanue, *Proc. Natl. Acad. Sci.*, 1982, 79, 175-178.

- 43 L. H. Wang, K. G. Rothberg and R. G. Anderson, J. Cell. Biol., 1993, 123, 1107–1117.
- 44 M. L. Elkjaer, H. Birn, P. Agre, E. I. Christensen and S. Nielsen, *Eur. J. Cell. Biol.*, 1995, **67**, 57-72.
- 45 S. Y. Lim, K. H. Hong, D. I. Kim, H. Kwon and H. J. Kim, *J. Am. Chem. Soc.*, 2014, **136**, 7018-7025.
- 46 Y. C. Chen, C. C. Zhu, Z. H. Yang, J. J. Chen, Y. F. He, Y. Jiao, W. J. He, L. Qiu, J. J. Cen and Z. J. Guo, *Angew. Chem. Int. Ed.*, 2013, **52**, 1732-1735.
- 47 X. H. Tian, M. R. Gill, I. Cantón, J. A. Thomas and G. Battaglia, Chen. Bio. Chem., 2011, 12, 548-551.
- 48 M. R. Gill, D. Cecchin, M. G. Walker, R. S. Mulla, G. Battaglia, C. Smythe and J. A. Thomas, *Chem. Sci.*, 2013, **4**, 4512-4519.

A novel phenanthroline Ru (II) derivative to targeting mitochondrial DNA was designed and highlight its potential applications in biological processes.

